

Fracture toughness of the fibre–matrix interface in glass–epoxy composites

A. PEGORETTI*, M.L. ACCORSI‡, A.T. DIBENEDETTO

Department of Chemical Engineering and Institute of Materials Science, and ‡ Department of Civil Engineering, University of Connecticut, Storrs, CT 06269, USA

The failure process arising at a broken fibre end in polymer matrix composite materials has been studied experimentally and analytically using the finite element method. A series of experiments were carried out using S-glass and E-glass single filaments, with different sizings and/or coupling agents, embedded in epoxy matrices with different moduli. A finite element analysis was used to simulate the experiments and calculate the change in strain energy accompanying the observed fracture mode. The strain energy release rate upon arrest of the crack, G_{arrest} , was then calculated. The measured interface debonding energies varied from $G_{\text{arrest}} = 57\text{--}342 \text{ J m}^{-2}$, depending primarily on the nature of the fibre sizing and the ratio of moduli of the fibre and matrix. Transverse and shear matrix cracks were characterized by G_{arrest} values of $58\text{--}103 \text{ J m}^{-2}$. Subtle changes in the constituent properties or fibre surface treatment resulted in a change in the fracture mode. This measurement and analysis technique may suggest reasons for the variability of previous measurements of interfacial adhesion, and provide a standard method for characterizing fracture modes at broken fibre ends.

1. Introduction

The mechanical properties of fibre reinforced composites strongly depend on the efficiency of stress transfer between matrix and fibre [1–5]. During recent years a great deal of effort has been expended to characterize the fibre–matrix interactions, and several experimental methods have been developed to measure the interfacial strength in polymeric composite materials [6, 7]. The most common methods involve micromechanical tests, such as the “embedded-single fibre composites” (SFC) test [8, 9] and a variety of single-fibre pull-out [10], microdebond [11] and microindentation [12] tests. A recent round-robin programme has shown that large differences exist in the reported values between different tests, and even within the same test technique [13]. It is, therefore, difficult to assess the utility of these parameters as a characterization property.

Data reduction using the different micromechanical tests has usually been based on the evaluation of an “interfacial shear stress”, τ , obtained from theories based on a pure shear stress field (e.g. shear lag theory). In the SFC test, for example, a single filament is embedded in a matrix and the specimen is placed under tension. At a specific level of strain, the fibre will break when the stress transferred through the matrix equals the fibre strength. Further breaks are induced until the fragments are too short to allow the transfer

of a stress higher than their breaking strength. This point is defined as the saturation of the fragmentation process. Various methods [8, 14, 15] have been used to extract an interfacial shear strength value from the mean fragment length at saturation, all of which are based on a force equilibrium. To characterize the maximum stress transferability, a number of authors [16–23] have recently proposed several alternative ways based on the evaluation of the mechanical energy required to decouple a fibre from the matrix.

To understand better the significance of results obtained from an SFC test, one must have information concerning the fracture behaviour at or near the fibre/matrix interface. When a continuous filament is fractured, the stored energy lost in the region around the fibre break is usually sufficient to generate fractures in the matrix and/or along the interphase. Three modes of failure are commonly observed, namely, a disc-shaped matrix crack perpendicular to the fibre, two inclined conical matrix cracks emanating from both broken fibre ends, and an interphase crack running parallel to the fibre surface. Combinations of these fracture patterns have also been observed.

The objective of this study was to measure the strain energy release rate at arrest, G_{arrest} , associated with each observable fracture mode using a combination of experimental observations and computer simulation of the process. The effects of composite constituent

* Permanent address: Department of Materials Engineering, University of Trento, via Mesiano 77, 38050 Trento, Italy.

properties and interfacial adhesion on its magnitude, were considered. A series of experiments were carried out using S-glass and E-glass single filaments treated with different sizing and/or coupling agents embedded in epoxy matrices of different moduli. Samples were mounted under an optical microscope and loaded until a single fibre fracture occurs. The strain at break was monitored and, at constant strain, the fracture emanating from the broken fibre end was observed and its dimensions measured. The MARC finite element code was used to simulate the experiments and calculate the change in the elastic strain energy accompanying the observed fracture mode. The strain energy release rate upon arrest of the crack, G_{arrest} , was then calculated.

2. Experimental procedure

2.1. Materials

Embedded single fibre composite specimens were made using the following matrices and fibres.

Stiff epoxy: diglycidyl ether of bisphenol-A (DER 331, Dow Chemical) cured with 14 p.h.r. by weight of tetra-ethylene-pentamine (DEH 26, Dow Chemical).

Soft epoxy: a mixture of 70/30 by weight of DER 331 and diglycidyl-ether of propylene-glycol (DER 732, Dow Chemical) cured with 11.5 p.h.r. by weight of DEH 26.

S-glass fibres (Owens Corning), with an average diameter of 10 μm . These fibres were supplied with two different surface treatments, the first being a starch coating and the second a commercial epoxy-compatible sizing. The starch-coated fibres were either used as-received or ultraviolet–ozone cleaned for 1 h [24]. The cleaned (bare) fibres were then surface treated in two different ways.

Some of the fibres were coated with an epoxy resin mixture 50/50 by weight of DER 331 and DER 732 cured with 10 p.h.r. by weight of DEH 26 from a solution of 0.3 wt/vol% epoxy resin in acetone. The bottom of a glass petri dish was filled with the coating solution and the fibres were added for a period of 5 min. The fibres were then removed from the solution and allowed to dry in air for a period of 10 min, after which they were placed into a vacuum oven and dried at room temperature under vacuum for 30 min. The oven was brought up to atmospheric pressure, and the epoxy resin coating was cured at 80 °C for 2 h. The remaining ultraviolet–ozone-cleaned fibres were coated with methyl-trimethoxy-silane (United Chemical Technology). The silane was applied by immersing the fibres for 5 min in a primer solution of 5% silane and 5% water in 90% methanol by volume. After removal from the primer solution, the fibres were dried in air for 10 min and then placed in an oven at 100 °C for 30 min.

Water-sized E-glass fibres (Union Carbide), with an average diameter of 13 μm . These fibres were ultraviolet–ozone cleaned for 0.5 h in order to remove organic impurities. Some of the ultraviolet–ozone-cleaned E-glass fibres were coated with methyl-trimethoxy-silane following the same procedure described above for the S-glass fibres.

2.2. Embedded-single fibre test

The specimens for the SFC test were prepared by placing a single glass fibre along the centreline of an ASTM D-638 type V silicone mould using adhesive tape. The catalysed resin was slowly poured into the dog-bone shaped mould to fill the cavity. All visible air bubbles in the gauge area of the sample were then carefully removed or moved to the ends of the mould. All the samples were cured for 1 h at 80 °C, slowly cooled in an oven and carefully removed from the silicone mould.

The SFC samples were tested using a handheld microtensile tester which used a hand-turned screw-type mechanism for stretching the sample. This unit was mounted on to a high-powered transmission optical microscope and the SFC sample was slowly pulled until the first fibre break was observed. The strain in the sample gauge length was measured by monitoring the relative displacement between two scored markers, using the calibrated eyepiece of the microscope. In this way the strain at first fibre break was determined. Crossed polarized light was used to observe the birefringence patterns at fibre break. At a power magnification of $\times 400$, a detailed fracture pattern analysis was carried out at constant strain by measuring the dimensions of arrested cracks emanating from the broken fibre ends. At least five specimens were tested for each experimental situation.

2.3. Strain energy release rate evaluation

The change in elastic strain energy associated with the observed fracture patterns was evaluated by using a linear elastic, axisymmetric finite element method (FEM) in a way similar to that previously reported by DiBenedetto *et al.* [16], by Di Anselmo *et al.* [18], and by Jones and DiBenedetto [22]. The FEM code used in this study was MARC (MARC Analysis Research Corporation). The embedded single-fibre specimen was modelled as a cylinder of matrix material surrounding a glass fibre (Fig. 1). Simulation was carried out on one quadrant of the cylinder with (AB) and (AFE) as the axes of symmetry. The half-length of the fibre (AB) was 50 μm and the outer radius of the cylinder (BD) was 30 μm . The outer radius dimension was chosen sufficiently large to allow the stresses to

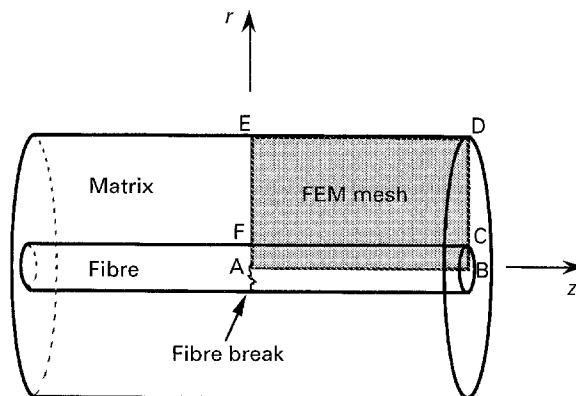


Figure 1 Schematic drawing of the region (ABDE) considered for the FEM analysis.

return to a uniform field. The fibre radius (AF) was 5 μm for the S-glass fibres and 6.5 μm for the E-glass fibres. No slippage between fibre and matrix and linear elastic behaviour were assumed. The following boundary conditions were applied to the FEM model:

- (i) side AB: displacement equal to zero in the r direction;
- (ii) side BCD: prescribed uniform displacement in the z direction;
- (iii) side DE: free surface;
- (iv) sides AFE: displacement equal to zero in the z direction.

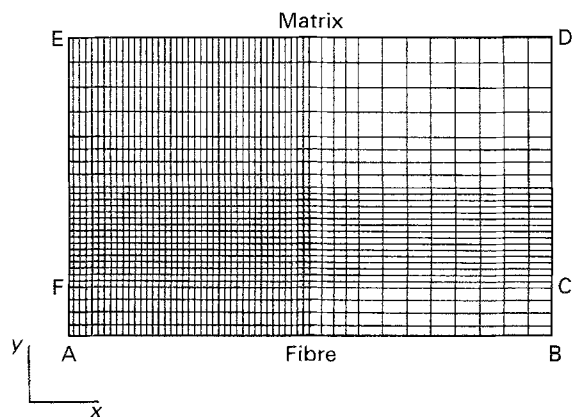
Fibre breakage was simulated by releasing the boundary condition in the side (AF) to produce a free fibre surface. The matrix and fibre mechanical properties used for the FEM simulation are reported in Table I.

TABLE I Composites constituent materials properties used for the FEM analysis

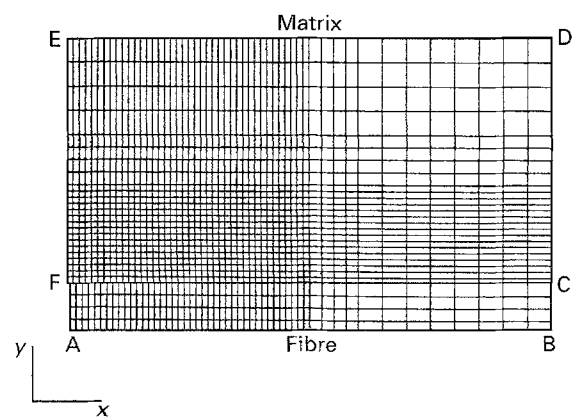
Material	Tensile modulus, E (GPa)	Poisson's ratio, ν
Stiff epoxy ^a	2.9	0.35
Soft epoxy ^a	1.6	0.35
S glass fibre ^b	86.9	0.22
E glass fibre ^b	72.0	0.22

^a Values taken from [22].

^b Data taken from an Owens Corning technical report.



(a)

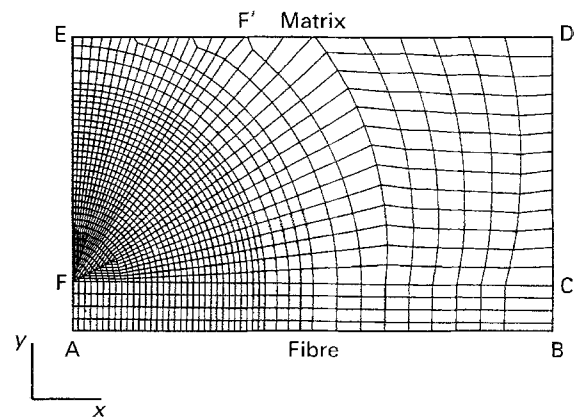


(b)

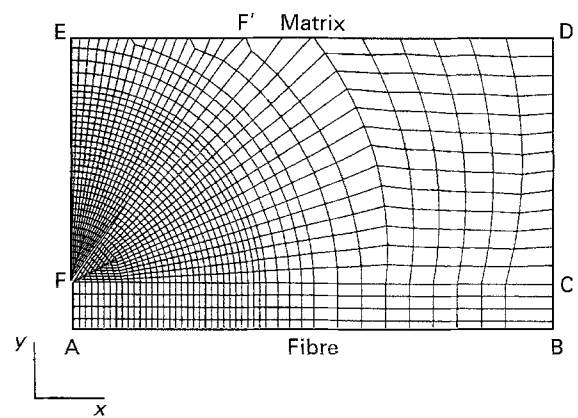
Figure 2 (a) Undeformed and (b) 0.01 strain deformed finite element mesh used for modelling a 10 μm interfacial crack.

Different crack patterns were simulated by deleting appropriate mesh elements or by using suitable boundary conditions.

The model used for interfacial debonding is shown in Fig. 2a and b which represent the undeformed model before fibre fracture and the deformed (strain equal to 0.01) configurations after fibre fracture, respectively. An interfacial crack was simulated by introducing a discontinuity (20 μm) between the fibre and matrix elements using duplicate nodes along the line FC. By progressively connecting the duplicate interfacial nodes, it is possible progressively to reduce the interfacial crack length from 20 μm to 0 μm . The same mesh was used for analysing the transverse matrix crack. A matrix crack perpendicular to the fibre was simulated by releasing the displacement boundary condition at appropriate nodes along the side EF of the model. The undeformed and the deformed (strain equal to 0.01) configurations of the model used for analysing the conical matrix crack are shown in Fig. 3a and b, respectively. The conical matrix crack was simulated by introducing a discontinuity (15 μm) in the matrix elements using duplicate nodes along the line FF' which forms an angle with the fibre axis which has been experimentally determined. In all the cases studied, the angle was equal to 55°. By progressively connecting the duplicate nodes, it is possible to reduce the shear matrix crack length from 15 μm to 0 μm .



(a)



(b)

Figure 3 (a) Undeformed and (b) 0.01 strain deformed finite element mesh used for modelling a 10 μm shear matrix crack.

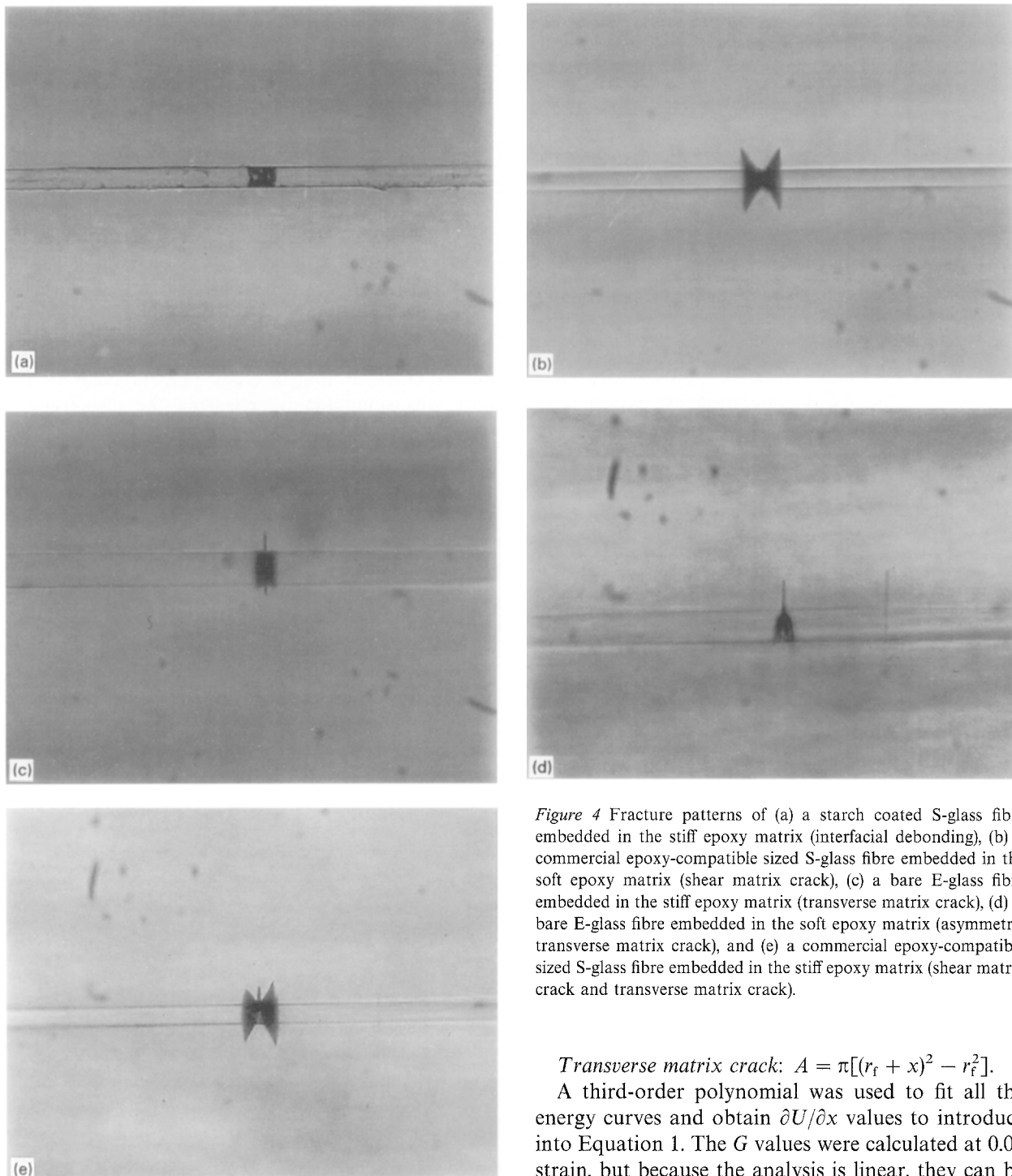


Figure 4 Fracture patterns of (a) a starch coated S-glass fibre embedded in the stiff epoxy matrix (interfacial debonding), (b) a commercial epoxy-compatible sized S-glass fibre embedded in the soft epoxy matrix (shear matrix crack), (c) a bare E-glass fibre embedded in the stiff epoxy matrix (transverse matrix crack), (d) a bare E-glass fibre embedded in the soft epoxy matrix (asymmetric transverse matrix crack), and (e) a commercial epoxy-compatible sized S-glass fibre embedded in the stiff epoxy matrix (shear matrix crack and transverse matrix crack).

Transverse matrix crack: $A = \pi[(r_f + x)^2 - r_f^2]$.

A third-order polynomial was used to fit all the energy curves and obtain $\partial U/\partial x$ values to introduce into Equation 1. The G values were calculated at 0.01 strain, but because the analysis is linear, they can be scaled to any other ε strain values by using the following relationship

$$G_\varepsilon = \left(\frac{\varepsilon}{0.01}\right)^2 G \quad (2)$$

where G_ε is the strain energy release rate corresponding to a strain ε .

From the FEM analysis, a plot of the total stored elastic strain energy, U , as a function of the crack length, x , can be constructed. A strain energy release rate, G , was then determined from the relationship

$$G = -\frac{\partial U}{\partial A} = -\frac{\partial U}{\partial x} \frac{\partial x}{\partial A} \quad (1)$$

where A is the crack area. For each of the three different fracture patterns, the crack area can be computed as a function of the crack length, x , as follows.

Interfacial debonding: $A = 2\pi r_f x$, where r_f is the fibre radius.

Shear matrix crack: $A = \pi(2r_f x + x^2 \sin \alpha)$, where α is the angle between the conical crack surface and the fibre axis.

3. Results and discussion

The fracture patterns at the broken fibre end were dependent on the matrix-fibre combination and on the interphase properties. Interfacial debonding is characterized by a crack running parallel to the fibre surface, either along the interface or in the matrix phase very close to the fibre surface (i.e. in the inter-phase) (Fig. 4a). It occurred as the primary mode of

failure in most of the stiff matrix microcomposites, except when using the bare E-glass fibres. It was also the primary mode of failure in soft matrix microcomposites, except when using the commercial epoxy-compatible sized or bare S-glass fibres.

Shear matrix cracks are characterized by two conical-shaped cracks emanating from both the broken fibre ends (Fig. 4b). These occurred in the soft matrix microcomposites reinforced with the bare and commercial epoxy-compatible sized S-glass fibres. The angle between the crack surface and the fibre axis was always approximately equal to 55° .

As reported in Fig. 4c, the stiff matrix microcomposites reinforced with bare E-glass fibre are characterized by a disc-shape crack propagating perpendicular to the fibre axis (transverse matrix crack). Most often only a semicircular crack was propagated in the matrix (Fig. 4d), most likely as a result of an asymmetric stress concentration in the fracture zone, perhaps, for example, as the result of a non-perfect fibre alignment along the sample centreline. In some cases, the occurrence of a mixed fracture pattern, such as simultaneous shear and transverse crack, have been observed (Fig. 4e). These last two cases have not been considered for the strain energy release rate evaluation.

A schematic illustration of the fracture patterns analysed using the FEM analysis is shown in Fig. 5, where L_d , L_s , and L_t , represent the interfacial debonding length, the shear matrix crack length, and the transverse matrix crack length, respectively. The strain at first fibre break and the dimensions of the fracture patterns observed for various matrix–fibre combinations and fibre surface treatments are reported in Table II. For the starch, soft epoxy, and methyltrimethoxy-silane sized S-glass fibres and for the methyltrimethoxy-silane sized E-glass fibres, interfacial debonding has been experimentally observed both with the stiff and soft epoxy matrices. For microcomposites reinforced with commercial epoxy-compatible silane sized S-glass fibre, bare S and E-glass fibres, shear or transverse matrix cracking occur instead of interfacial debonding. An important observation is that the S-glass fibres have an average strain at break equal to 5.2% compared to only 2.4% for the E-glass fibres. As a consequence, the elastic strain energy stored in the system before the first fibre fracture is higher for the S-glass reinforced composites than for the E-glass fibre system.

Plots of the elastic strain energy release rate as a function of the crack length for the four matrix–fibre combinations obtained by simulation using the FEM analysis, are shown in Fig. 6a–d. By using these curves and the experimental data reported in Table II, we obtained the elastic strain energy release rate at crack arrest, G_{arrest} , for each observable fracture. The G_{arrest} values for the various matrix–fibre and interphase combinations are reported in Table III. The G_{arrest} values for the interfacial debonding are in the range $57\text{--}342\text{ J m}^{-2}$. These values are in good agreement with other experimental results obtained from different energy-based approaches to the matrix–fibre debonding. For an E-glass fibre system, DiBenedetto

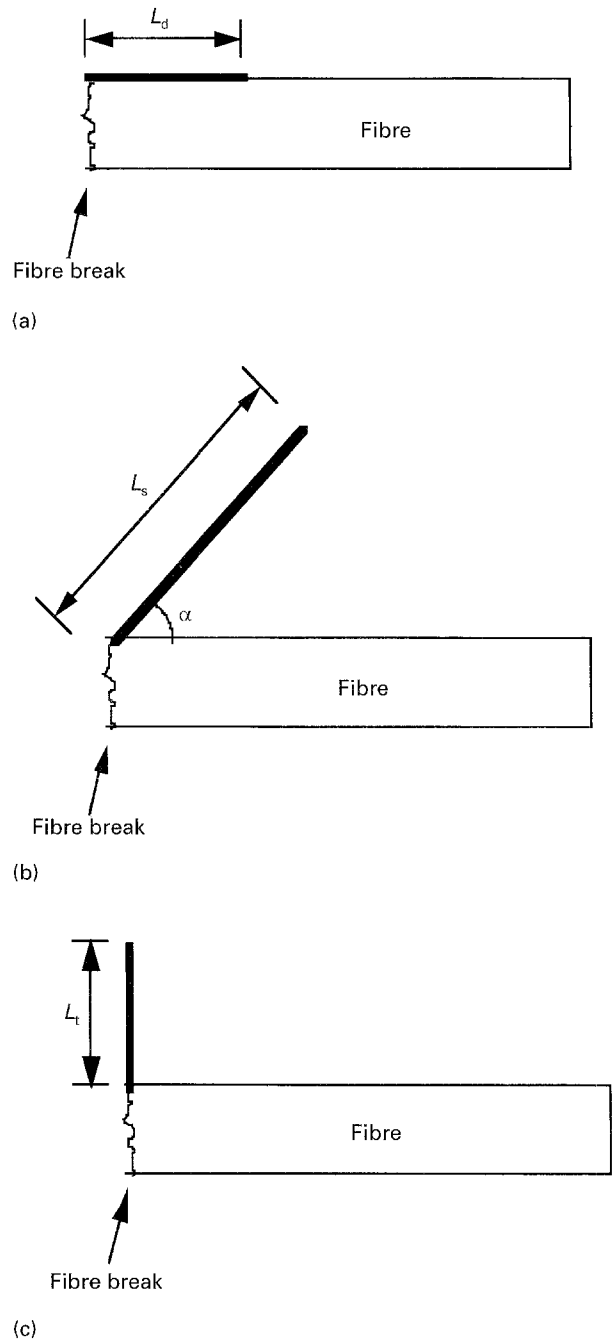


Figure 5 Schematic illustration of the crack dimensions experimentally measured for the various fracture patterns. (a) Interfacial debonding, (b) shear matrix cracking, (c) transverse matrix cracking.

[17] reported debonding fracture energies of the order of 60 J m^{-2} for poorly bonded interfaces, to 230 J m^{-2} for well-bonded interfaces. Wagner *et al.* [20] evaluated interface energies for the initiation of debonding equal to 264 and 183 J m^{-2} , respectively, for sized and unsized E-glass fibre embedded in an ultraviolet-cured urethane matrix. Similar fracture mechanics approaches for measuring the interfacial toughness with the microbond test led to similar results. Scheer and Nairn [21] reported an interfacial fracture toughness of about 220 J m^{-2} for debonding of epoxy resin droplets on E-glass fibres. Analysing a single-fibre pull-out test on an E-glass fibre–polycarbonate matrix, Hampe and Marotzke [23] determined an interfacial energy release rate from $70\text{--}130\text{ J m}^{-2}$.

TABLE II Experimentally measured strain for the first fibre break and fracture pattern dimensions for various matrix–fibre and interphase combinations. The significance of L_d , L_s and L_t is shown in Fig. 5

Epoxy/glass	Fibre surface treatment	Strain at first break (%)	Mode of failure and crack length (μm)
Stiff/S	Starch	5.2 ± 0.5	Interfacial debonding $L_d = 5.6 \pm 0.3$
Stiff/S	Soft epoxy coating	4.8 ± 0.4	Interfacial debonding $L_d = 5.5 \pm 0.6$
Stiff/S	Methyltrimethoxysilane	4.6 ± 0.3	Interfacial debonding $L_d = 9.4 \pm 1.0$
Soft/S	Starch	6.1 ± 0.7	Interfacial debonding $L_d = 9.2 \pm 1.0$
Soft/S	Soft epoxy coating	5.8 ± 0.6	Interfacial debonding $L_d = 9.3 \pm 0.8$
Soft/S	Methyltrimethoxysilane	5.1 ± 0.4	Interfacial debonding $L_d = 14.2 \pm 2.3$
Soft/S	Commercial epoxy compatible sizing	5.5 ± 0.4	Shear matrix crack $L_s = 11.3 \pm 1.1$
Soft/S	Bare	4.9 ± 0.4	Shear matrix crack $L_s = 12.0 \pm 1.3$
Stiff/E	Methyltrimethoxysilane	2.5 ± 0.2	Interfacial debonding $L_d = 3.9 \pm 0.6$
Soft/E	Methyltrimethoxysilane	2.4 ± 0.2	Interfacial debonding $L_d = 5.8 \pm 0.4$
Stiff/E	Bare	2.4	Transverse matrix crack $L_t = 4.8^a$

^a Single experimental result.

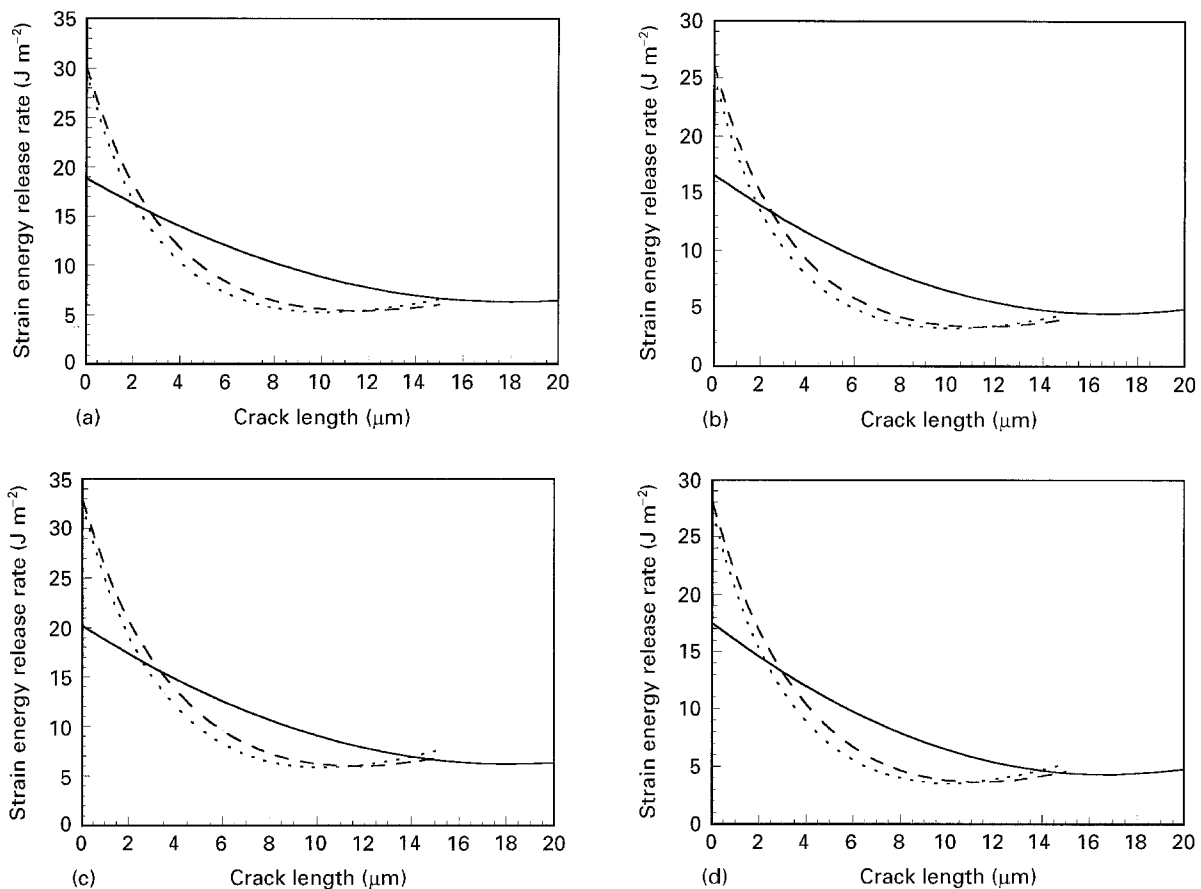


Figure 6 Strain energy release rate as a function of the crack length for various fracture patterns: (a) stiff epoxy–S-glass system; (b) soft epoxy–S-glass system; (c) stiff epoxy–E-glass system; (d) soft epoxy–E-glass system. (—) Interfacial debonding, (---) shear matrix cracking, (- - -) transverse matrix cracking.

The experimental data indicate that the interfacial fracture toughness for a composite with a specific fibre surface treatment, as measured by the G_{arrest} value, is always higher for the stiff matrix composites com-

pared to those with the soft matrix. A similar behaviour has been reported for the interfacial shear strength by Asloun *et al.* [25] and Rao and Drzal [26]. For various polymer matrix composites, these authors

TABLE III G_{arrest} values for various matrix–fibre and interface combinations

Epoxy/glass	Fibre surface treatment	Fracture pattern	G_{arrest} (J m^{-2})
Stiff/S	Starch	Interfacial debonding	342 ± 68
Stiff/S	Soft epoxy coating	Interfacial debonding	281 ± 48
Stiff/S	Methyltrimethoxysilane	Interfacial debonding	198 ± 23
Soft/S	Starch	Interfacial debonding	261 ± 48
Soft/S	Soft epoxy coating	Interfacial debonding	233 ± 55
Soft/S	methyltrimethoxysilane	Interfacial debonding	127 ± 21
Soft/S	Commercial epoxy compatible sizing	Shear matrix crack	103 ± 12
Soft/S	Bare	Shear matrix crack	84 ± 12
Stiff/E	Methyltrimethoxysilane	Interfacial debonding	94 ± 10
Soft/E	Methyltrimethoxysilane	Interfacial debonding	57 ± 11
Stiff/E	Bare	Transverse matrix crack	58 ^a

^a Single experimental result.

found that the interfacial shear strength increased with increasing matrix modulus. When methyl-trimethoxysilane, a releasing agent, was used to coat the S-glass fibres, we obtained the lower G_{arrest} values for interfacial debonding, as expected and as previously reported [27].

The shear and transverse matrix cracking G_{arrest} values were in the range from 58–103 J m^{-2} . It is interesting to observe that for an epoxy resin (DER 332) similar to the cured matrix used in this work, Mostovoy and Ripling [28] found that the measured mode I fracture toughness, G_{Ic} , as a function of the curing agent (tetra-ethylene-pentamine) ranged from 70–100 J m^{-2} .

When one compares the elastic strain energy release rate, G_{arrest} , for interfacial debonding using the same matrix and the methyl-trimethoxy-silane fibre sizing treatment, but different fibres, one finds that the S-glass fibre system results in calculated values of G_{arrest} that are higher by approximately two times that of the E-glass fibre system. The modulus of elasticity of the S-glass is about 1.2 times higher than that of the E-glass, and its strain-to-break is approximately 2.1 times higher than E-glass. Thus, the strain energy stored in the fibre prior to the first fibre fracture is approximately 5.3 times (1.2×2.1^2) higher in the S-glass fibre. The apparent increase in interfacial fracture toughness may be caused by one or all of the following three factors.

1. Because there is a difference between the chemical composition of the two glass fibres, there is a difference in the work of adhesion with the epoxy matrix. Nardin and Schultz reported the following relation between work of adhesion and the interfacial shear stress [29]

$$W_A = \lambda \tau \left(\frac{E_f}{E_m} \right)^{\frac{1}{2}} \quad (3)$$

where W_A is work of adhesion, λ is a characteristic intermolecular distance, τ is the shear strength of the interface in an SFC test and (E_f/E_m) is the ratio of the fibre and the matrix moduli.

From a molecular interaction analysis, one can show that the work of adhesion is also related to the

work of cohesion of the matrix material near the interface by the following equation [30]

$$W_A = \zeta_R W_C \left(\frac{E_f}{E_m} \right)_i^{\frac{1}{2}} \quad (4)$$

where ζ_R is a dimensionless reduced intermolecular distance parameter, W_A is work of adhesion, W_C is work of cohesion and $(E_f/E_m)_i$ is the ratio of the theoretical maximum moduli of the fibre and the matrix near the interface. In light of the fact that the sizing thickness is of the order of nanometres, it is not expected that this factor can account for the large difference in the G_{arrest} values.

2. The interfacial debonding occurs in a complicated multicomponent stress field and thus should be described in terms of a combined mode I and mode II displacement. The FEM calculation of the ratio of the tensile component (mode I) to the shear component (mode II) near the crack tip shows that the relative shear component is about 15% higher in the S-glass system. Thus, this factor may account for part of the difference in the G_{arrest} values.

3. After the fibre fractures, there is a radial compression imposed on the fibre end caused by the expansion of the fibre diameter and the contraction of the matrix around the fibre end due to Poisson's effects and an increase in the level of strain locally in the matrix. Fig. 7a–d show the results of the finite element analysis of the shear and radial stresses around the crack tips in the two cases considered, using a technique for maintaining contact of the mesh points at the debonded surfaces. The radial stresses were found to be independent of the magnitude of the friction coefficient utilized in the analysis. We emphasize, however, that the analysis is dependent on the mesh geometry and thus gives only a crude estimate of the stress gradients.

Within these limitations, one sees that the fibre/matrix interfaces behind the crack tips still support shear and compressive radial stresses. As a crack tip advances, the fibre behind the tip retracts to a fraction of the initial strain under a frictional force generated by the radial stress. We used a friction coefficient of

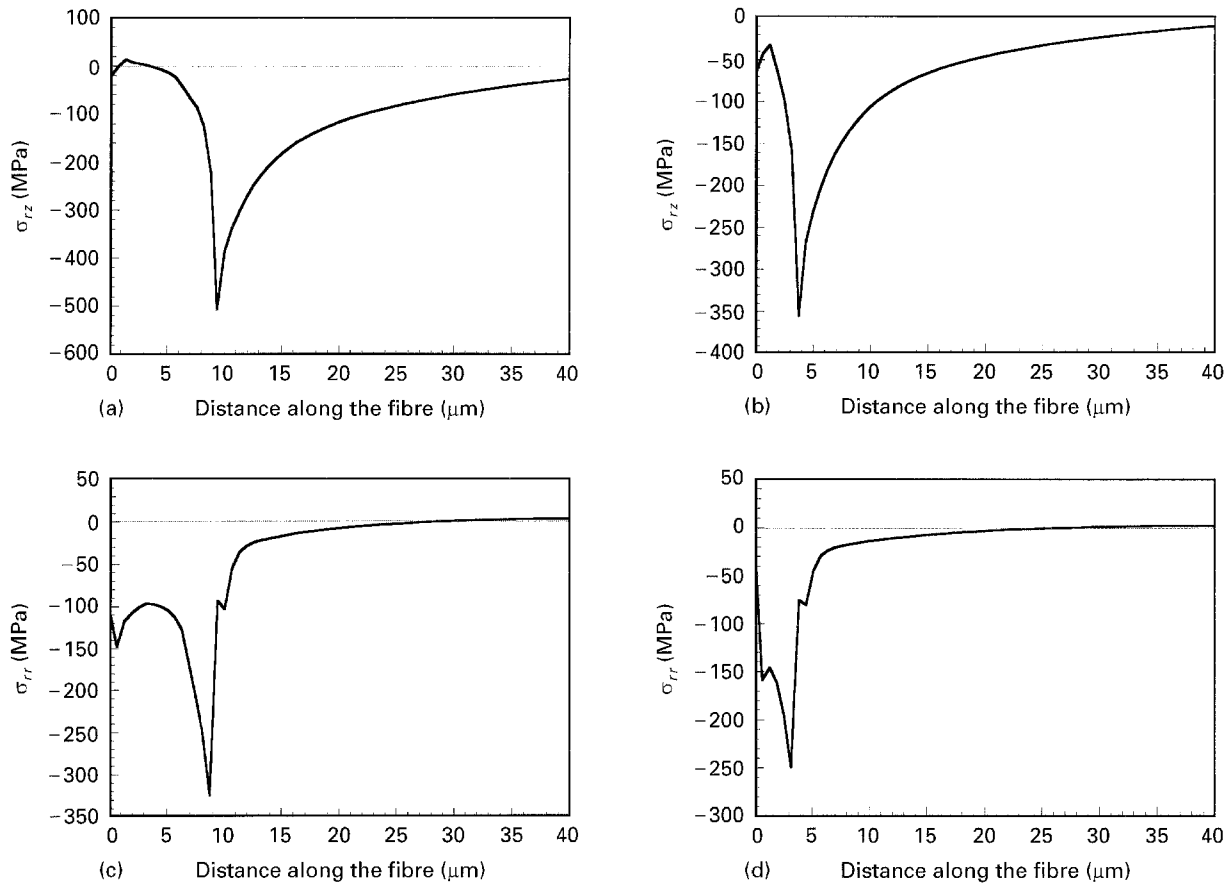


Figure 7 (a) Shear stress along the surface of an S-glass fibre embedded in the stiff epoxy matrix. The FEM model contains a 9.4 μm interfacial crack and is deformed at a strain of 0.046. (b) Shear stress along the surface of an E-glass fibre embedded in the stiff epoxy matrix. The FEM model contains a 3.9 μm interfacial crack and is deformed at a strain of 0.025. (c) Radial stress along the surface of an S-glass fibre embedded in the stiff epoxy matrix. The FEM model contains a 9.4 μm interfacial crack and is deformed at a strain of 0.046. (d) Radial stress along the surface of an E-glass fibre embedded in the stiff epoxy matrix. The FEM model contains a 3.9 μm interfacial crack and is deformed at a strain of 0.025.

$\mu = 1.2$, (as measured by Wu for a glass fibre-reinforced epoxy composite laminate [31]), to estimate the frictional work done during retraction of the fibre end.

Fig. 7a and b show maximum shear stresses of about 500 and 350 MPa at the crack tips of the S-glass and E-glass composites, respectively. The shear stresses decrease rapidly towards 0–50 MPa as one moves toward the fibre ends. We estimate that under these conditions the fibre ends behind the crack tips will retract approximately 50–75% of the original strain prior to filament fracture. The work done against friction is estimated to be:

$$W_{\text{friction}} = \mu \sigma_{rr} l_c (\Delta \epsilon) \quad (5)$$

where μ is the frictional coefficient, σ_{rr} is the compressive radial stress, l_c is the crack length and $(\Delta \epsilon)$ is the change of the strain from the original level.

Fig. 7c and d show maximum compressive radial stresses of 325 and 250 MPa behind the advancing crack tips of the S-glass and E-glass composites, respectively. Using these maxima in Equation 5, one obtains values of 84–127 J m^{-2} for the frictional work in the S-glass composite and 15–22 J m^{-2} for the frictional work in the E-glass composite. Subtracting the higher values from the total G_{arrest} values of 198 and 94 J m^{-2} (Table III), one obtains a residual value of 72 J m^{-2} for the debonding energy in the two composites, which is of the order of magnitude of the

G_{arrest} values for the observed shear matrix cracks. Using the lower values for the frictional work, one obtains a residual value of 114 J m^{-2} for the debonding energy in the S-glass composite and 80 J m^{-2} for the debonding energy in the E-glass composite. As stated previously, these values are within the range of fracture toughness found by Mostovoy and Ripling for similar epoxy resins [28]. Within the level of confidence of the analysis, it appears to us that the G_{arrest} values for debonding consist primarily of the sum of the fracture energy of the matrix in the vicinity of the interface and the work of friction associated with the retraction of the broken fibre ends.

4. Conclusion

In this study, an experimental method for evaluating the strain energy release rate at crack arrest, G_{arrest} , associated with various fracture patterns at the broken fibre end of polymeric composite materials, has been assessed. A series of experiments have been carried out using S-glass and E-glass single filaments with different sizing and or coupling agent treatments embedded in epoxy matrices of different moduli. An axisymmetric finite element analysis was used to simulate the experiments and evaluate the change in strain energy accompanying the observed fracture mode. When a fibre filament breaks, cracks have been

observed to propagate from the broken fibre end either by interfacial debonding, shear conical matrix cracks, transverse matrix cracking, or a combination of the three modes. We have measured interfacial debonding energies varying from 57–342 Jm⁻², depending primarily on the nature of the fibre sizing and the ratio of moduli of the fibre and matrix. When the adhesion is weak, the higher breaking strain of the S-glass fibre composite provides a higher interface debonding energy, 194 Jm⁻² compared to 57–93 Jm⁻² when E-glass is used. Transverse and shear matrix cracks were characterized by G_{arrest} values of 58–103 Jm⁻². Subtle changes in the constituent properties of fibre surface treatment resulted in a change in the fracture mode. This measurement and analysis technique may suggest reasons for the variability of previous measurements of interface adhesion and provide a standard method for characterizing fracture modes at a broken fibre end.

References

1. L. DILANDRO, A. T. DIBENEDETTO and J. GROEGER, *Polym. Compos.* **9** (1988) 209.
2. M. S. MADHUKAR and L. T. DRZAL, *J. Compos. Mater.* **25** (1991) 932.
3. *Idem, ibid.* **25** (1991) 958.
4. *Idem, ibid.* **26** (1992) 310.
5. *Idem, ibid.* **26** (1992) 936.
6. P. J. HERRERA-FRANCO and L. T. DRZAL, *Composites* **23** (1992) 2.
7. M. NARKIS and J. H. CHEN, *Polym. Compos.* **9** (1988) 245.
8. W. A. FRASER, F. H. ANCKER and A. T. DIBENEDETTO, in "Proceedings of the 30th Annual Technical Conference" (Reinforced Plastics/Composites Institute, The Society of the Plastics Industry Inc., Washington D.C., 1975) Section 22-A, p. 1.
9. L. T. DRZAL, M. J. RICH, J. D. CAMPING and W. J. PARK, in "Proceedings of the 35th Annual Technical Conference" (Reinforced Plastics/Composites Institute, The Society of the Plastics Industry Inc., Washington D.C., 1980) Section 20-C, p. 1.
10. M. R. PIGGOTT, P. S. CHUA and D. ANDISON, *Polym. Compos.* **6** (1985) 242.
11. B. MILLER, P. MURI and L. REBENFELD, *Compos. Sci. Technol.* **28** (1987) 17.
12. J. F. MANDELL, D. H. GRANDE, T. H. TSIANG and F. J. MCGARRY, in "Proceedings of the 7th International Conference on Composite Materials: Testing and Design", ASTM STP 893, edited by J. M. Whitney (American Society for Testing and Materials, Philadelphia, PA, 1986) p. 87.
13. M. J. PITKETHLY, J. P. FAVRE, U. GAUR, J. JAKUBOWSKI, S. F. MUDRICH, D. L. CALDWELL, L. T. DRZAL, M. NARDIN, H. D. WAGNER, L. DILANDRO, A. HAMPE, J. P. ARMISTEAD, M. DESAEGER and I. VERPOEST, *Compos. Sci. Technol.* **48** (1993) 205.
14. R. B. HENSTENBURG and S. L. PHOENIX, *Polym. Compos.* **10** (1989) 389.
15. L. T. DRZAL, M. J. RICH and P. F. LLOYD, *J. Adhes.* **16** (1983) 1.
16. A. T. DIBENEDETTO, S. M. CONNELLY, W. C. LEE and M. L. ACCORSI, *ibid.* **52** (1995) 41.
17. A. T. DIBENEDETTO, *Compos. Sci. Technol.* **42** (1991) 103.
18. A. DI ANSELMO, M. L. ACCORSI and A. T. DIBENEDETTO, *ibid.* **44** (1992) 215.
19. H. D. WAGNER and S. LING, *Adv. Compos. Lett.* **2**(5) (1993) 169.
20. H. D. WAGNER, J. A. NAIRN and M. DETASSIS, *Appl. Comp. Mater.* **2** (1995) 107.
21. R. J. SCHEER and J. A. NAIRN, *J. Adhes.* **53** (1995) 45.
22. K. D. JONES and A. T. DIBENEDETTO, in "Proceedings of the 3rd International Conference on Deformation and Fracture of Composites", Guildford, UK, March 1995, p. 86.
23. A. HAMPE and C. MAROTZKE, *ibid.* p. 132.
24. S. RANADE and A. T. DIBENEDETTO, presented at EUDAH '96, Churchill College, Cambridge, 3–6 September, 1996.
25. E. L. M. ASLOUN, M. NARDIN and J. SCHULTZ, *J. Mater. Sci.* **24** (1989) 1835.
26. V. RAO and L. T. DRZAL, *Polym. Compos.* **12** (1991) 48.
27. A. T. DIBENEDETTO and P. J. LEX, *Polym. Eng. Sci.* **29** (1989) 543.
28. S. MOSTOVOY and E. J. RIPLING, *J. Appl. Polym. Sci.* **10** (1996) 1351.
29. M. NARDIN and J. SCHULTZ in "The Interfacial Interactions in Polymeric Composites", edited by G. Akevali (Kluwer Academic, The Netherlands, 1993) p. 94.
30. A. T. DIBENEDETTO, personal communication (September, 1995).
31. E. WU, in "Composite Materials", Vol 5, "Fracture and Fatigue", edited by L. J. Broutman and R. H. Kroch (Academic Press, New York, HBJ Publishers, 1974) p. 191.

Received 3 January
and accepted 18 March 1996